ARL-TR-8848 ● Nov 2019

DEVCOM ARMY RESEARCH LABORATORY

Scientific Development and Characterization of a Soft Armor Inspection System for Body and Vehicle Ballistic Armor: Phase I Final Report

by Tyrone Jones, Brian Scott, Robert Haynes, Russell Austin, Reza Zoughi, Mohammad Tayeb Ghasr, and John Gallion

NOTICES

Disclaimers

The findings in this report are not to be construed as an official Department of the Army position unless so designated by other authorized documents.

Citation of manufacturer's or trade names does not constitute an official endorsement or approval of the use thereof.

Destroy this report when it is no longer needed. Do not return it to the originator.

ARL-TR-8848 ● Nov 2019

Scientific Development and Characterization of a Soft Armor Inspection System for Body and Vehicle Ballistic Armor: Phase I Final Report

Tyrone Jones and Brian Scott
Weapons and Materials Research Directorate, CCDC Army Research Laboratory

Robert Haynes
Vehicle Technology Directorate, CCDC Army Research Laboratory

Russell Austin
Texas Research Institute Austin, Inc.

Reza Zoughi, Mohammad Tayeb Ghasr, and John Gallion
Electrical and Computer Engineering Department,
Missouri University of Science and Technology

REPORT DOCUMENTATION PAGE			Form Approved OMB No. 0704-0188

1. REPORT DATE *(DD-MM-YYYY)*	2. REPORT TYPE	3. DATES COVERED (From - To)
November 2019	Technical Report	15 July 2017–25 July 2019

4. TITLE AND SUBTITLE
Scientific Development and Characterization of a Soft Armor Inspection System for Body and Vehicle Ballistic Armor: Phase I Final Report

5a. CONTRACT NUMBER

5b. GRANT NUMBER

5c. PROGRAM ELEMENT NUMBER

6. AUTHOR(S)
Tyrone Jones, Brian Scott, Robert Haynes, Russell Austin, Reza Zoughi, Mohammad Tayeb Ghasr, and John Gallion

5d. PROJECT NUMBER
W911QX-17-P-0167

5e. TASK NUMBER

5f. WORK UNIT NUMBER

7. PERFORMING ORGANIZATION NAME(S) AND ADDRESS(ES)
CCDC Army Research Laboratory*
ATTN: FCDD-RLW-PE
Aberdeen Proving Ground, MD 21005

8. PERFORMING ORGANIZATION REPORT NUMBER
ARL-TR-8848

9. SPONSORING/MONITORING AGENCY NAME(S) AND ADDRESS(ES)

10. SPONSOR/MONITOR'S ACRONYM(S)

11. SPONSOR/MONITOR'S REPORT NUMBER(S)

12. DISTRIBUTION/AVAILABILITY STATEMENT
Approved for public release; distribution is unlimited.

13. SUPPLEMENTARY NOTES
* As of February 2019, the US Army Research Laboratory has been renamed the US Army Combat Capabilities Development Command Army Research Laboratory (CCDC ARL).

14. ABSTRACT
Composite body armors are subjected to extreme in-service and environmental stresses, such as *extreme* temperature changes. Evaluating body armor property (e.g., materials and thickness), in particular variations of thickness from its nominal value, is of great interest. Microwave nondestructive testing and evaluation techniques (NDT&E), using open-ended rectangular waveguide probes have been successfully developed and used for evaluating materials' properties and thickness in stratified composite structures, which are similar to a body armor, and even those that are significantly more complex in design. Microwave NDT&E techniques have improved and advanced over a period of more than two decades during which the efficacy of the analytical formulations and measurement tools significantly increase the accuracy associated with this type of evaluation. This technique was used in this study to evaluate body armor properties. Additionally, the efficacy of the "wideband frequency-modulated continuous-wave" radar approach was demonstrated (on a limited basis) to illustrate its potential utility for thickness evaluation.

15. SUBJECT TERMS
Digital Terrain Model, DTM, microwave nondestructive testing and evaluation techniques, NDT&E, waveguide, thickness evaluation, radar, body armor, soft armor, thermal degradation

16. SECURITY CLASSIFICATION OF:			17. LIMITATION OF ABSTRACT	18. NUMBER OF PAGES	19a. NAME OF RESPONSIBLE PERSON
a. REPORT	b. ABSTRACT	c. THIS PAGE			Tyrone Jones
Unclassified	Unclassified	Unclassified	UU	51	19b. TELEPHONE NUMBER (Include area code) (410) 278-6223

Contents

List of Figures

List of Tables

1. Introduction

Shortly after fielding the Enhanced Small Arms Protective Insert (ESAPI) plates, a number of the plates were taken out of service due to failing the Armor Inspection System (AIS) testing. Program Executive Office Soldier contacted the US Army Research Laboratory* (ARL) to investigate the failures and help assess whether the ballistic failures in the soft armor were stochastic or the result of a systemic design flaw. This is a primary objective of the Physics of Soldier Protection Essential Research Program.

Current inspection capabilities require armor to be removed from the troops or vehicles and sent to higher maintenance levels, often out of theater, for testing. Chesapeake Testing (Belcamp, Maryland) introduced a computed tomography (CT) X-ray scanner system in 2012 to inspect the construction of the material in the battlefield.[1] This CT X-ray scanner provides dual 225- and 450-kV microfocus panel scan capability allowing scans of objects up to 37 inches wide. However, the scanner requires a higher level maintenance facility and is not suitable for battlefield settings.

The Smart Body Armor technology was a Small Business Innovation Research (SBIR)-funded project in 2008 to University of California, Irvine professor Maria Feng. This led to the subsequent development of Smart Body Armor technology by Newport Sensors Inc. (Irvine, California) and acquisition in October 2014 by TenCate (The Netherlands).[2–4] The Smart Body Armor technology provides real-time ability of delamination detection between the ceramic and back plates of body armor systems. However, the Smart Body Armor technology is limited to ceramic materials and unable to detect delaminations in composites. The Smart Body Armor technology can only test embedded fiber optic sensors in ceramic body armor plates.

The SBIR project, *In-Service Technique for Assessing Conditions of Ballistic Protective Inserts in Personnel Armor,* was awarded to the Physical Acoustics Corporation (Princeton Junction, New Jersey), and was funded for Phases I and II of the project from 2004–2007. The project applied acoustic emission testing.[5] However, the system was not fielded, as it was unable to establish a statistically sound pass/fail criterion. Therefore, it was not suitable for battlefield settings.

Lastly, in 2008 there was an experimental project for performing lock-in IR inspection that used IR thermography to evaluate areas of internal damage in

* As of February 2019, the US Army Research Laboratory has been renamed the US Army Combat Capabilities Development Command Army Research Laboratory (CCDC ARL).

ballistic-protection composite samples.[6] This technique provided nondestructive testing (NDT) of composite armors by using IR thermographic methods. However, the technique is experimental and not field portable. It is believed that the limitations are related to ballistic protection thickness and the type of materials used in manufacturing the composites.[7,8]

The limitations of these systems have the potential for delaying replacement armor and depend upon additional logistical support, which creates supplementary manpower requirements and supply issues. Any delay in providing replacement armor for combat Soldiers has a potentially negative effect on survivability issues. Additionally, there are significant material and labor costs for unnecessarily replacing serviceable armor.

Personnel and vehicle ballistic armors are composed of multilayer, soft composite structures of various combinations of glass, ceramic, Kevlar, ultra-high-molecular-weight polyethylene (UHMWPE), and metal alloys, all prone to damage in handling and use. Relatively minor impacts could cause damage in a number of ways. Dropping the armor plate onto a hard surface or nonballistic impact (diving for cover, etc.) could fracture the ceramic, cause fiber/matrix damage in the retention layer, or delaminate any of the layers from their neighbors.

The US Army has the need for a ruggedized, portable device that can be easily transported and operated by a single Soldier that uses nondestructive inspection (NDI) techniques to reliably identify micro-deformations in soft composites up to 2-inches thick before they evolve into critical defects capable of threatening the structural integrity of the material and to detect weaknesses in adhesive bonds before they fail. The device must work on both flat and curved surfaces. Solutions that use X-rays will not be considered under this topic to avoid radiation effects and shielding requirements. The development of NDT must provide a solution in battlefield settings. The portable device should be powered by existing, rechargeable Army batteries and be capable of continuous operation for at least 1 h without changing batteries.

The interval objectives of the program are as follows:

Phase I:

Develop a system design that meets the previously stated objectives. Demonstrate through modeling, simulation, and/or laboratory experiments that the proposed design can identify micro-deformations and micro-cracking on flat and curved, monolithic and layered soft armor configurations with a 90% probability of success. Identify the NDI methods and demonstrate a proof-of-concept system that can be implemented in the Phase II prototype system.

Phase II:
Develop a prototype system that will meet the requirements defined in Phase I and permit usage in remote settings with no controlled environmental conditions. Initial testing will require soft armor pieces with various types and degrees of damage to provide statistically valid test results for calibrating a field portable unit. Demonstrate the device to identify micro-deformations and micro-cracking in soft composite materials with a 95% probability of success.

Phase III:

The proposed technology will be commercialized and transitioned to the similar applications in law enforcement and private security firms. This capability will enable the first responder organizations to quickly evaluate the condition of their body armor.

This report documents Phase I activities toward the development of a compact, rugged field-portable device weighing less than 20 lb that is capable of personnel armor NDI to enable rapid identification of defective armor while deployed in an active combat environment. The goal of this program is to provide a Department of Defense Technical Readiness Level of 6—system/subsystem model or prototype demonstration in a relevant environment—and transition this system directly to the US Army.

Texas Research Institute Austin, Inc. (TRI Austin) was selected to team with the ARL as of 15 June 2017 under contract W911QX-17-P-0167 to develop an NDI system for detecting damage in soft armor. The system will be based on low-power, nonionizing energy in the microwave/millimeter wave frequency bands.

2. Performance Report

In Phase I, Russell Austin, principal investigator from TRI Austin, traveled to ARL twice: once for the kickoff meeting and again to collect microwave NDE data on armor panels throughout thermal cycling. Details of the kickoff meeting are in the Appendix.

At different times in Phase I, the team evaluated a total of five different sample types in nine configurations from four manufacturers as follows:

1) TIVAR 1000 natural monolithic UHMWPE plate

2) Leading Technology Composites (LTC) of Wichita, Kansas
    a. Part Number 28340: large, alumina oxide ESAPI plate
        i. Qty 2, alumina Small Arms Protective Inserts (SAPI) with padding in front and back of plates, and fabric cover

ii. Qty 1, alumina SAPI with no padding and no cover

b. Part Number 28520: large, boron carbide ESAPI plate
   i. Qty 2, boron carbide SAPI with padding in front and back of plates, and fabric cover
   ii. Qty 1, boron carbide SAPI with no padding and no cover

3) SAPI plate made by manufacturer "b"
   a. b105, as-received from manufacturer
   b. b106, same part number as b105, but with padding and cloth cover removed

4) SAPI plate made by manufacturer "c"
   a. c105, as-received from manufacturer
   b. c106, same part number as c105, but with padding and cloth cover removed

3. Theoretical Background

Nonmagnetic dielectric materials (electrically nonconducting) are characterized by a complex parameter known as the dielectric constant,

$$\varepsilon = \varepsilon' - j\varepsilon''. \quad (1)$$

The real part, ε', is known as the permittivity and the imaginary part, ε'', is known as the loss factor. Permittivity indicates the ability of the material to store microwave energy, while loss factor indicates the ability to absorb microwave energy. The ratio of loss factor to permittivity is referred to as loss tangent ($tan\delta$). These two parameters are commonly referenced to the permittivity of free space, ε_0, resulting in *relative* complex dielectric constant given by[9]

$$\varepsilon_r = \varepsilon'_r - j\varepsilon''_r . \quad (2)$$

There are many methods in the microwave regime by which complex dielectric constant may be measured. However, it is important to note that ε (or ε_r) is an *intrinsic parameter* associated directly with the nature of the material and thus remains unchanged independent of the measurement method used to measure it.[10,11]

When microwave signals interact with layered dielectric composites, not only the signal in each layer undergoes an amplitude and phase change, but singular and multiple reflections at each boundary contribute to the total reflected-from and transmitted-through signals.[10] Figures 1a–b shows the general schematic of an electrically thick material (i.e., thick or made of a lossy dielectric material) and a structure composed of an arbitrary number of layers with different complex

dielectric constants and thicknesses consisting of multiple reflections within each layer, respectively.

There are a number of ways by which the reflected and transmitted-through signals may be measured for the case shown in Fig. 1b. The "free-space" or "transmission-through" measurement technique that is commonly used incorporates two antennas (probes), each placed on either side of the sample, and using a power-sensitive or vector-type measuring tool (e.g., a vector network analyzer [VNA]), the total transmitted signal power, its amplitude, and phase may be directly measured. Although this is a direct and straightforward technique, it does present several measurement-related issues such as the need for proper alignment of the two antennas, correctly accounting for reflection from the font surface, and so on. However, there are other robust measurement methods that only require a "reflection" measurement, which can provide information not only about the characteristics of the reflected wave, but also those of the transmitted wave (e.g., transmitted wave power level, or its signal amplitude and phase). Reflection measurement techniques are also much simpler to perform than transmission-through measurements.

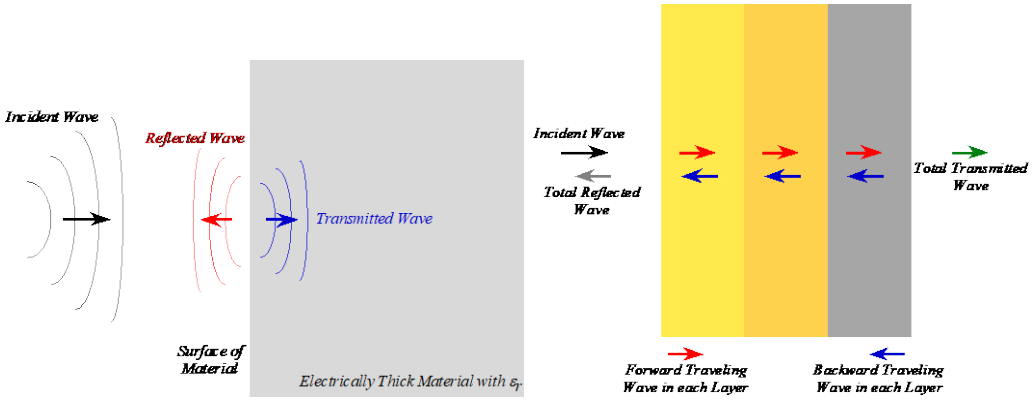

Fig. 1 Reflected and transmitted components of a wave incident upon a) an electrically thick material and b) a generally lossy layered composite structure

In the past two decades, significant electromagnetic model development and experimental works have been conducted in determining the interaction of open-ended rectangular waveguide probes with stratified composites made of an arbitrary number of layers, thicknesses, and dielectric properties, as shown in Fig. 2 specific to a generally designed body armor consisting of a foam padding, armor composite, and a backing material.[12–15] The forward model that was developed[4] gives the amplitude and phase of reflection coefficient at the waveguide aperture for a given number of layers, thicknesses, and dielectric properties of each layer and the

frequency of operation. Later the model was expanded for infinite half-space materials to include the influence of higher-order modes generated at the waveguide aperture. This improvement was significant since it allowed for a much more accurate recalculation (or estimation) of the complex dielectric properties of the infinite half-space.[16] This work was further expanded to not only include the influence of higher-order modes, but to also consider a general multilayer structure.[17,18] Figure 3 shows the chronological extension and enhancement of these works. This enhancement is directly related to the objectives of this proposed work. Finally, potential recalculation inaccuracies, related to the finite size of the waveguide flange, was overcome by using a patented engineered (modified) flange that while finite in size, electromagnetically mimics an infinite-size flange.[19] The efficacy of using this robust method for evaluating stratified composites has been well documented.[19,20]

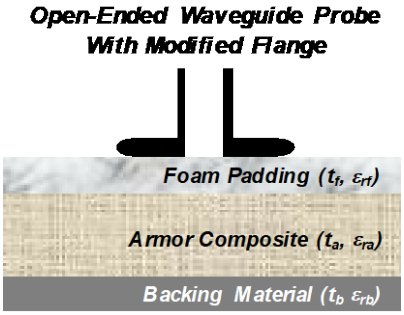

Fig. 2 Open-ended rectangular waveguide radiating into a stratified composite structure such as body armor (not to scale)

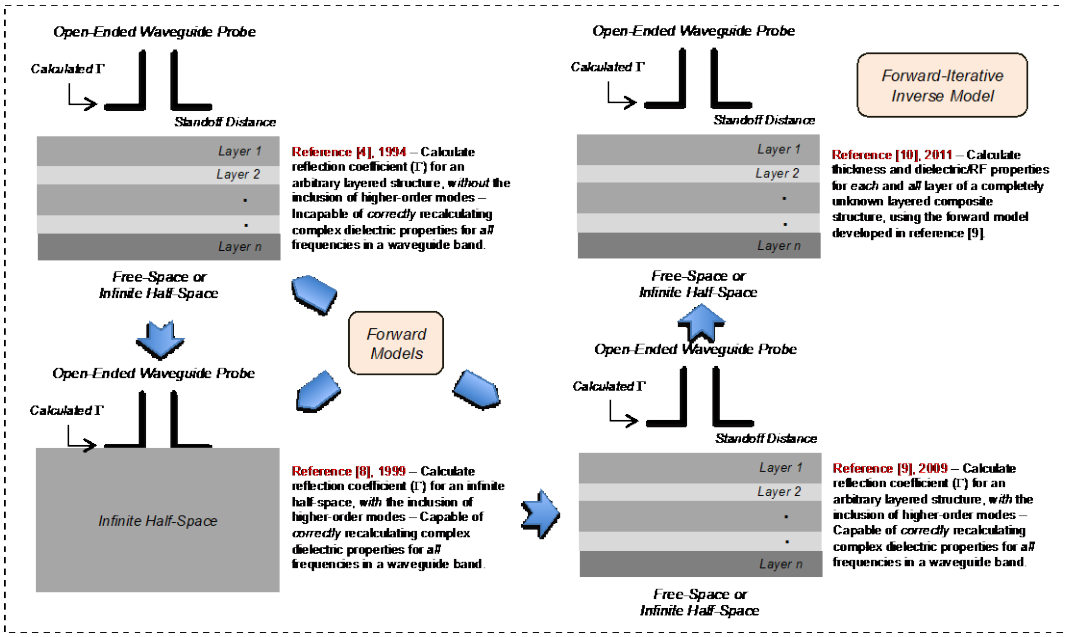

Fig. 3 Chronology of the development of a robust method to extract material thickness and dielectric/RF properties for each individual layer in a layered composite structure using open-ended waveguide probes

4. Evaluation of Sheet Material and Thickness (Inverse Problem)

To evaluate thickness and dielectric properties of one or all of the layers in the structure shown in Fig. 2, from the measurement of reflection coefficient (Γ_m) at a single or a wide band of frequencies, one must use an accurate and robust model that fully describes the forward problem, as the model does in Ghasr et al. (2009).[17] Given the complexity of the electromagnetic fields in the near-field of a waveguide probe interacting with a generally lossy layered structure, direct closed-form inversion of the model to estimate thicknesses and dielectric constants is not possible. However, owing to a robust and full-wave forward model,[17] we can use forward-iterative optimization techniques to explore different combinations of layer properties to achieve a close estimate between the measured and calculated reflection coefficient values. To use optimization techniques, first a proper cost function must be defined and then we can use a suitable minimum search technique. To perform the optimization, a proper cost-function definition is necessary. This approach was recently used to evaluate thickness and complex dielectric properties of a single layer of a multitude of layers (simultaneously), including the case of thin sheets.[17,18] Figure 4 shows the steps involved in this forward-iterative optimization technique.

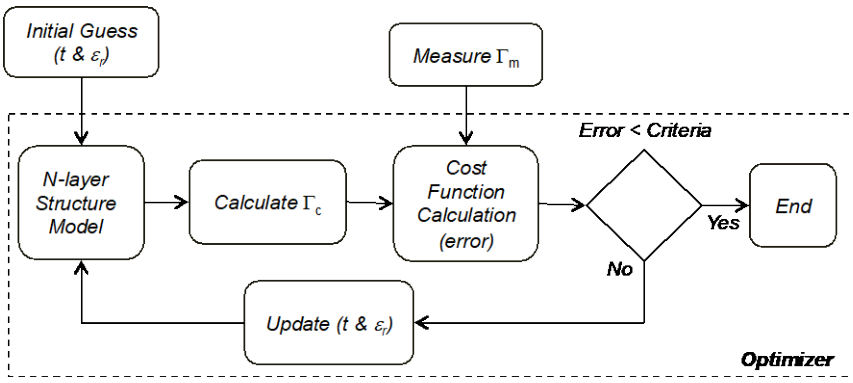

Fig. 4 Extraction of thickness and dielectric/RF properties of layers in a general layered composite using a forward-iterative optimization technique based on the robust full-wave forward model in Fallahpour et al.[18]

The cost-function used is (commonly) the square of the distance in the complex plane between the measured reflection coefficient and calculated reflection coefficient over the entire measurement bandwidth. For large numbers of layers and more unknowns, the time for calculating the unknown parameters could be long. However, when dealing with sheets whose nominal/expected thickness and dielectric property bounds are known, the estimation process can be made to be very fast.

While it is possible to determine the dielectric constant and the thickness of a material based on the reflection coefficient (as described previously), it is not always necessary to perform this process to detect changes in the materials and thickness properties of a stratified composite structure. The change in complex reflection coefficient, as a function of frequency, itself can be an effective indicator of such change.[21,22] This method also alleviates the need for potentially time-consuming forward-iterative calculation of materials and thickness properties. Both of these approaches were implemented in this work, as will be explained in the following sections.

5. Methodology

Initially, a series of tests were performed as an attempt to minimize the number of variables when determining changes in the shields (body armors) as a result of heating. Using similar materials as those used in the construction of body armors, we acquired several commercial off-the-shelf (COTS) sheets of UHMWPE. Using the open-ended rectangular waveguide method described earlier, and at Ka-band (26.5–40 GHz), the dielectric properties of the sheets were characterized. One sheet was subsequently subjected to several cycles of thermal heating and the experiments were repeated. Afterward, the same samples were measured again at

X-band (8.2–12.4 GHz) and Ku-band (12.4–18 GHz) to determine if the properties were similar to the values calculated at Ka-band (26.5–40 GHz). This initial investigation was quite useful in determining potential operating frequency for on-site measurements that were to be performed at Army facilities, and acquiring the proper handheld microwave VNA (i.e., Copper Mountain R180 [Copper Mountain Technologies, Indianapolis, Indiana]).

The next test was conducted on two different types of armor samples: 28340 and 28520. Manufactured by LTC, both types of panels were tested with and without the foam padding. Bulk samples of the alumina and the composite material were also measured along with the panels at Ku-band (12.4–18 GHz). Thicknesses of the materials allowed for direct calculation of the dielectric properties, which provided the missing parameters to estimate thicknesses of the panels with and without the foam padding. However, numerical issues were discovered in our model (for a portion of frequency range) that made it difficult to correctly model reflection coefficient of the panels. Thus, in addition to our model, a full-wave simulation was performed using CST Microwave Studio (CST MWS) (CST of America, Inc., Wellesley Hills, Massachusetts) to determine the thickness of the samples.

Extensive tests were also conducted measuring four unknown panels identified as b105, b106, c105, and c106 at the ARL Vehicle Technology Directorate in Building 4603. Complex reflection coefficient measurements were performed using the Copper Mountain VNA after each thermal cycle across six regions of each panel at Ku-band (12.4–18 GHz), some of which are reported here. The measurements were processed and the physical properties of the c106 were calculated.

Finally, limited wideband reflection properties were performed on some of the panels and the data were processed to give information similar to that of a wideband frequency-modulated continuous-wave (FM-CW) radar. We believe this type of processing is also informative for determining thickness variation in the panels, as will be discussed later.

6. Bulk Polyethylene (PE) Sample Dielectric Characterization

In this experiment, a 12- × 12- × 0.5-inch piece of plastic (TIVAR 1000 natural UHMWPE plate) was cut into four equally sized square pieces of approximately 6 × 6 inches. One piece of the sample was put in an oven to be heated while the rest were left in room temperature as control samples. For heating purposes, the oven temperature was first brought up to the desired level. Then the sample was placed in the oven and held at that temperature for 4 h before being taken out and performing microwave reflection measurements. After heating, the piece was removed immediately and its reflection coefficient was measured using the open-

ended rectangular waveguide method at Ka-band (26.5–40 GHz).[17] For every heating cycle, the same piece was heated inside of the oven with a thermometer measuring the temperature inside of the oven. Every time that the heated reflection coefficient of the "oven" sample was measured, the reflection coefficient of the other three (control) pieces that were left in room temperature were also measured. Ten different locations across the sample surface were measured in each case and the average and standard deviation of the measurements and subsequent recalculated thickness and dielectric properties are reported here. After collecting the measured reflection coefficient data, the method in Ghasr et al. [17] was used to calculate thickness and/or dielectric constant of the samples. Figure 5 shows a picture of the sample and the heating apparatus, respectively.

Fig. 5 Bulk PE sample (left); oven and thermometer (right)

Three different temperature levels were selected for this investigation (120, 140, and 160 °F) to investigate the level of expansion as a function of temperature over a period of time. The sample was first placed in an oven when the temperature was 120 °F, and it was left in that constant temperature for 4 h, as mentioned earlier. Then, the sample was removed and its reflection properties were immediately measured. This process was repeated two additional times to give a total of 30 data series for this temperature. The same procedure was repeated for 140 and 160 °F. However, for the latter temperature the sample was immediately placed in the oven to be heated at 160 °F for two more hours. After the additional 2 h of heating, the reflection properties were measured again. This resulted in 20 series of measurements for 160 °F.

Figures 6 and 7 show the calculated thickness, permittivity (real part of dielectric constant), and loss factor (imaginary part of dielectric constant) recalculated from the measured reflection coefficient data for the three samples that were left at room temperature (cool), and the one that was heated successively to 120, 140, and then 160 °F.

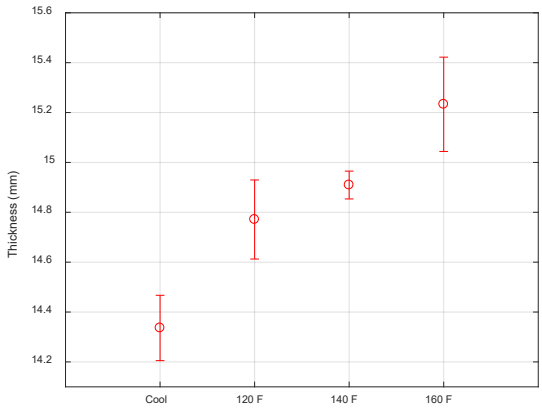

Fig. 6 Calculated thickness from reflection coefficient measurements for different temperatures

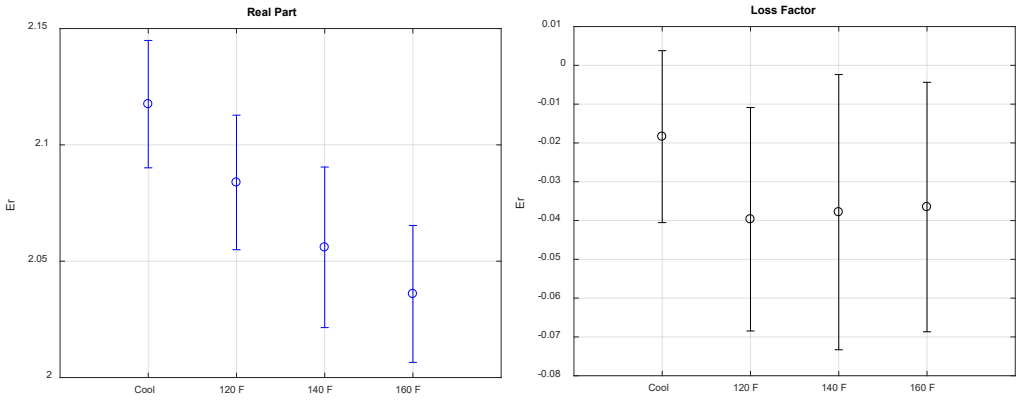

Fig. 7 Calculated dielectric properties of the PE sample: permittivity (left), and loss factor (right) after the baseline, 120, 140, and 160 °F tests

To reaffirm the previous findings, we reheated the same sample to 160 °F again and recalculated its dielectric properties and thickness. The sample was placed in the oven at 160 °F for 3 h. It was taken out and its thickness was immediately measured with a caliper in four locations. After the reflection coefficient of the heated sample was measured, it was placed on a metal rack to cool. The three samples that were never heated were measured once more. Finally, the sample that had been cooling was measured again.

Figure 8 shows the physically measured (with caliper) and calculated thickness of the never-heated cool samples (cool), the sample that had been previously heated at room temperature (room temp), the heated sample after it cooled to a temperature between the room temperature and 160 °F (warm), and the sample that was heated at 160 °F (heated). The difference in thickness between corresponding data points

is approximately 0.6 mm. Figure 9 shows the calculated complex dielectric properties of these samples.

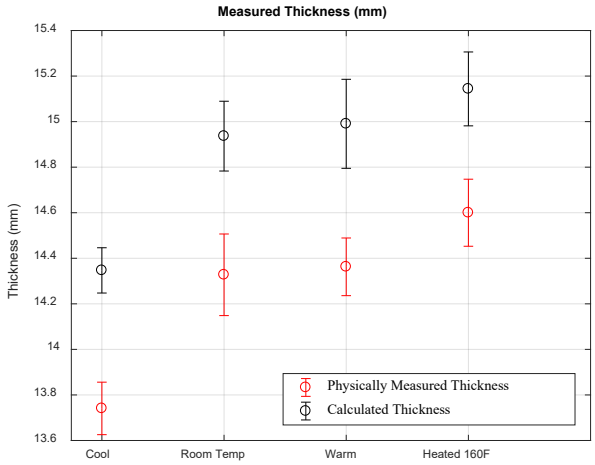

Fig. 8 Calculated thickness from reflection coefficient measurements for the repeated 160 °F test on the PE sample

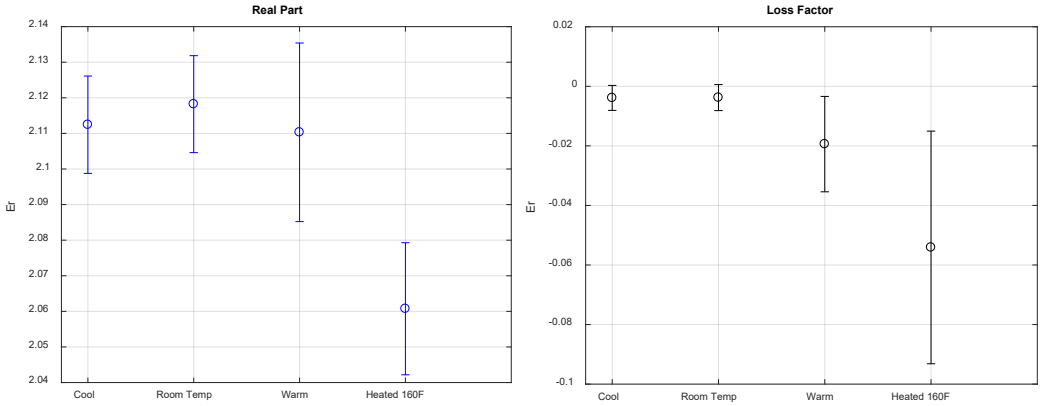

Fig. 9 Calculated dielectric properties of the PE sample: permittivity (left), and loss factor (right) for the repeated 160 °F test

Figure 10 shows the expanded view of the raw measured complex reflection coefficient. The three lines indicated as “cool” for the never-heated samples were measured, along with the initial 160 °F measurement of the heated sample. The “160 2” line are the data collected from the heated sample after an additional 2 h of being left in the 160 °F oven subsequent to an initial heating at 160 °F.

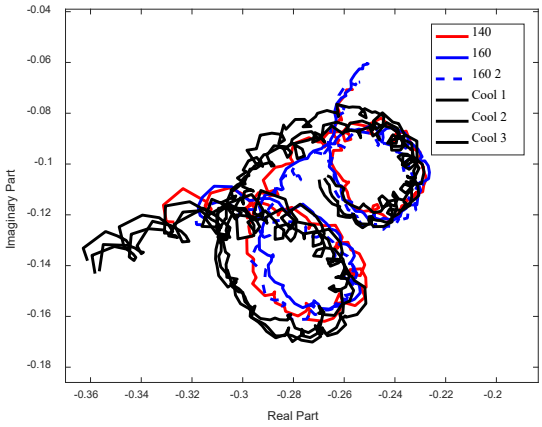

Fig. 10 Reflection coefficient before and after heating of the bulk PE sample

7. Armor Sample Characterization

In this experiment we used the six armor plates manufactured by LTC. Two samples (one with alumina and the other with boron carbide construction) had the foam padding and cloth cover removed. The four other samples (two each of the alumina and the boron carbide construction) had the foam padding and cloth cover in place. LTC also provided three pieces of scrap material: PE composite material, a piece of alumina, and a piece of boron carbide. The boron carbide sample is highly conductive at the microwave frequencies and cannot be penetrated, so it will act as a reflector to our energy. This can be helpful because it allowed our team to isolate the PE composite material. The other two samples were measured at Ku-band (12.4–18 GHz) and the dielectric constant of both was calculated. The results are in Table 1.

Table 1 Calculated dielectric constants for individual components of the shield

Sample	Alumina	PE composite
$\varepsilon_r = \varepsilon'_r - j\varepsilon''_r$	9.55-j0.01	2.3-j0.01

Next, Ku-band (12.4–18 GHz) and X-band (8.2–12.4 GHz) measurements were performed on the six armor samples on multiple locations in the inner side (UHMWPE composite side) of the samples shown in Fig. 11. This was done since the boron carbide is conductive and the alumina was covered by a conductive (carbon-based) film, hence blocking signal penetration from the front (outside) of the armor samples. The measured complex reflection coefficient results (in polar format) are shown in Fig. 12 for X-band (8.2–12.4 GHz) and Fig. 13 for Ku-band (12.4–18 GHz). Due to the size of the probing aperture and the curvature of the

samples, the X-band (8.2–12.4 GHz) measurements were performed on only three points of the samples while the Ku-band (12.4–18 GHz) measurements (smaller probe) were performed on five points. For future testing it is possible to design probes capable of matching a curved surface to allow for better matching to sample curvatures (as will be shown through numerical simulations later). These figures show that multiple measurements on a single sample are similar, while there is substantial difference between the measurements of different constructions. Calculation of physical parameters was attempted on these samples but a numerical issue caused inaccuracies in the modeling code, as will be discussed in Section 8. As these samples were not aged or changed in any way, no further analysis was conducted using open-ended waveguide measurement of dielectric properties.

Fig. 11 Image of samples: 28340 bare (left), 28340 covered #2 (middle), and 28520 covered #2 (right)

Sample 28340	Sample 28520
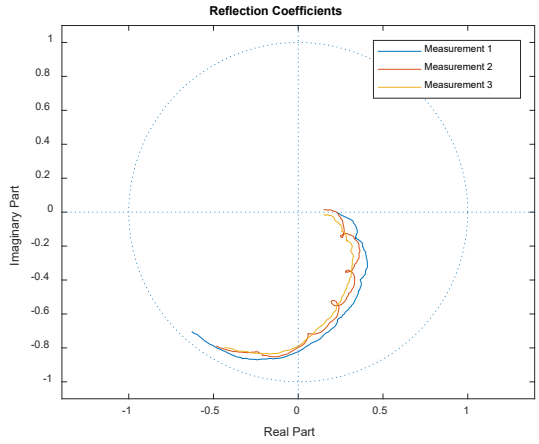	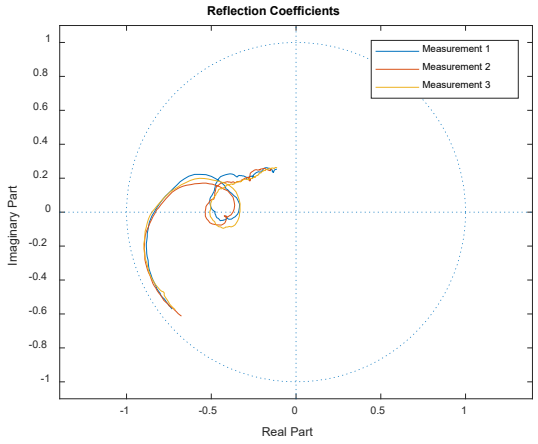
Bare Sample Back Side @ X-Band	Bare Sample Back Side @ X-Band
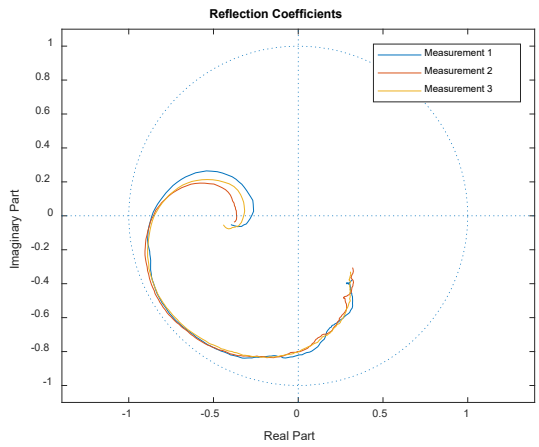	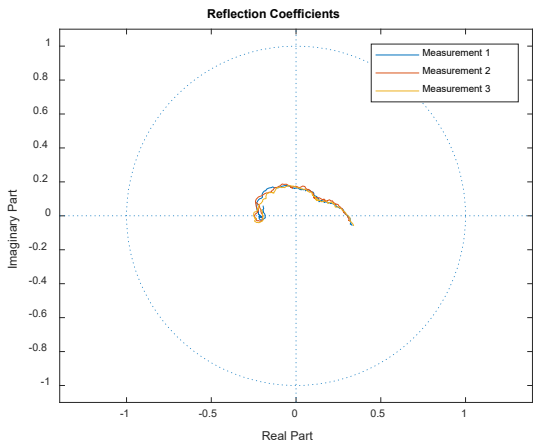
Covered Sample #1 Back Side @ X-Band	Covered Sample #1 Back Side @ X-Band
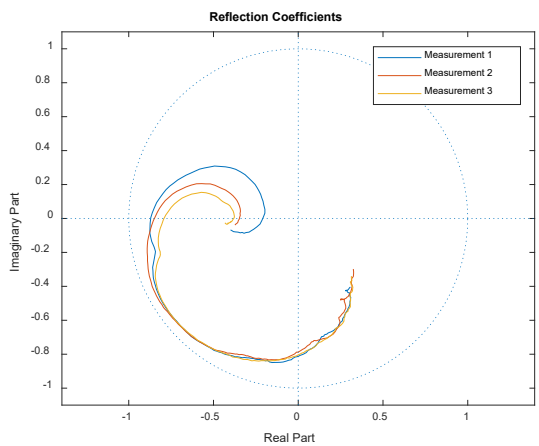	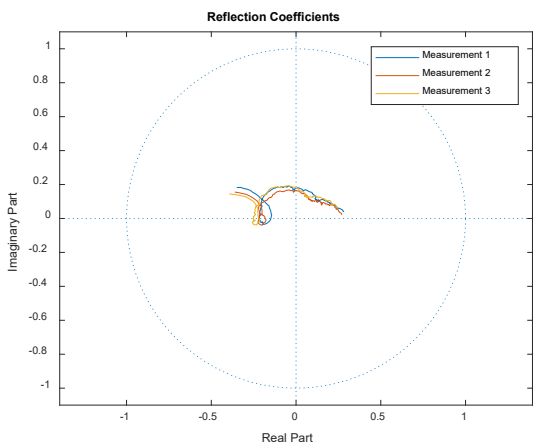
Covered Sample #2 Back Side @ X-Band	Covered Sample #2 Back Side @ X-Band

Fig. 12 Measured complex reflection coefficient results at center of the panel at X-band (8.2–12.4 GHz)

Sample 28340	Sample 28520
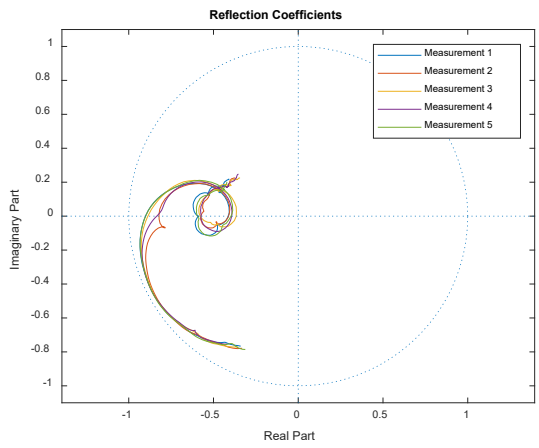	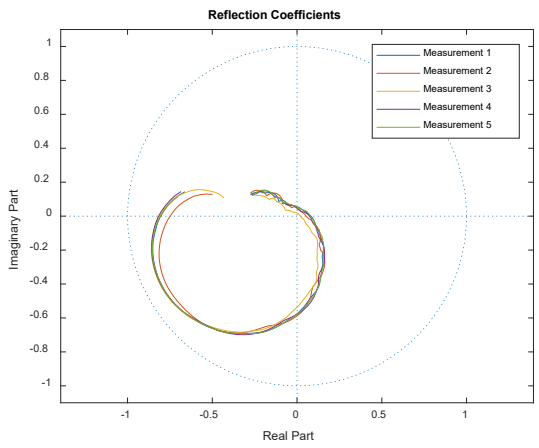
Bare Sample Back Side @ Ku-Band	Bare Sample Back Side @ Ku-Band
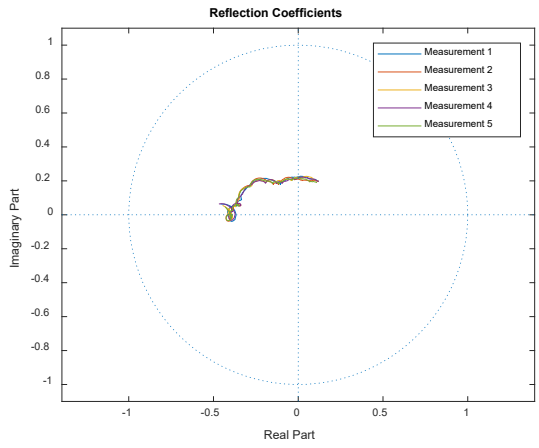	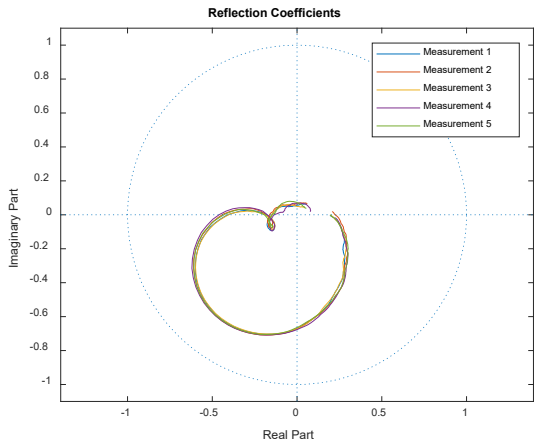
Covered Sample #1 Back Side @ Ku-Band	Covered Sample #1 Back Side @ Ku-Band
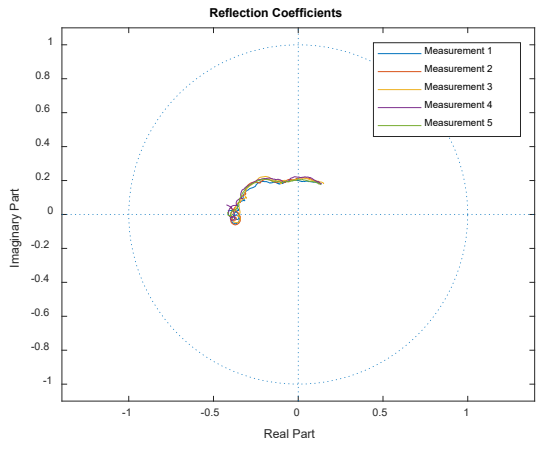	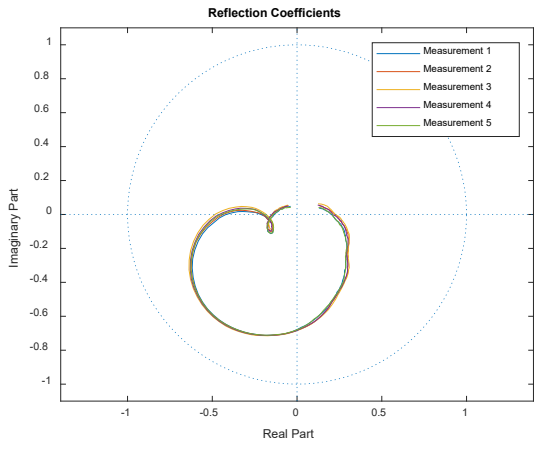
Covered Sample #2 Back Side @ Ku-Band	Covered Sample #2 Back Side @ Ku-Band

Fig. 13 Measured complex reflection coefficient results at center of the panel at Ku-band (12.4–18 GHz)

8. Army Experiments

The final test was conducted at the ARL Vehicle Technology Directorate in Building 4603. In total, four panels labeled b105, b106, c105, and c106 were measured through 21 thermal cycles. Two of the four panels had the foam padding (105 panels) while the other two had the foam padding removed (106 panels); the b105 and b106 panels are shown in Fig. 14. Measurements were taken on site with the Copper Mountain VNA at Ku-band (12.4–18 GHz). In all cases except for the first cycle the samples were heated for the duration of the cycle, then cooled before measuring. Measurements were taken in six designated regions, as shown in Fig. 14, over the entire sample. Two of the samples, b105 and c105, were measured with the foam padding still intact while the b106 and c106 samples only measured the composite layer backer. The differences in the reflection coefficients can be seen between the uncovered and covered (by the foam padding) samples in Fig. 15. If the dielectric constant and thickness of foam padding layer is accurately known, the method of calculating the thickness of the composite layer is unchanged from not having the foam padding.

Fig. 14 Panels b105 and b106 from the Army tests, including labeled regions

Sample B	Sample C
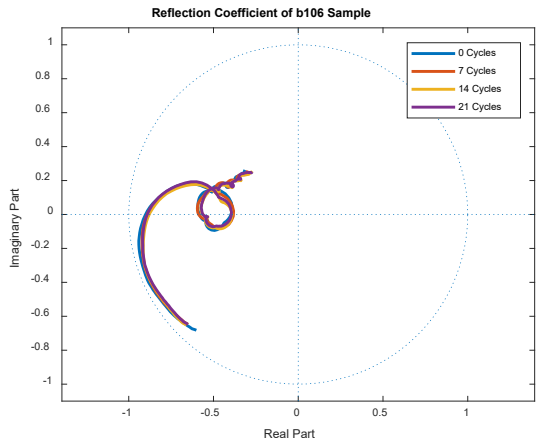	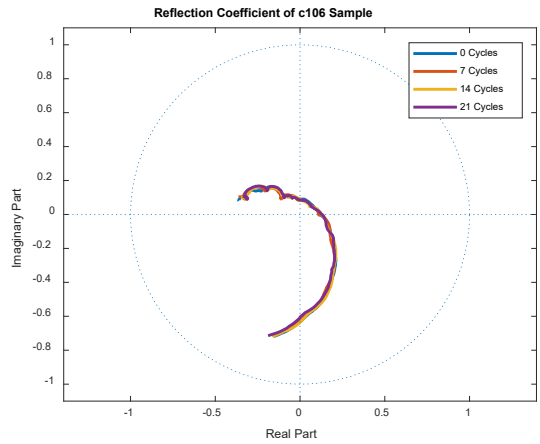
Reflection coefficient of the b106 sample	Reflection coefficient of the c106 sample
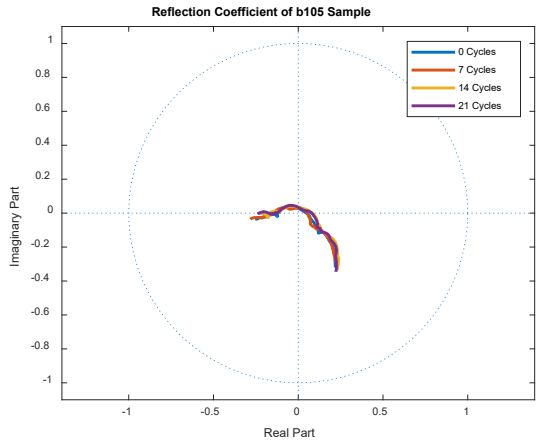	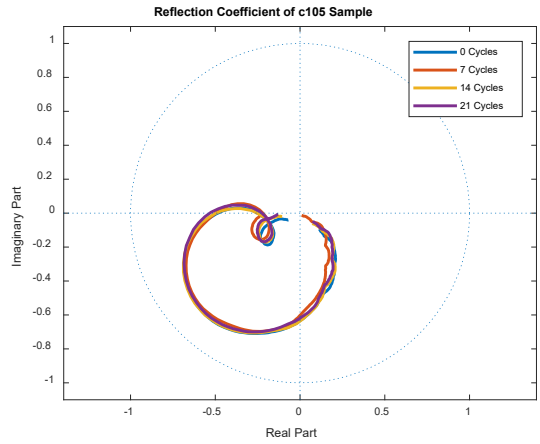
Reflection coefficient of the b105 sample	Reflection coefficient of the c105 sample

Fig. 15 Reflection coefficients for each sample over 0, 7, 14, and 21 cycles

Unfortunately, the numerical issue mentioned in Section 7 in our algorithm caused problems when trying to calculate the reflection coefficient of the panel, consequently the dielectric constant and thickness of the b106 samples could not be determined using the multilayered model. However, this numerical issue did not affect modeling of sample c106 and the resulting thickness following each cycle was calculated, as shown in Fig. 16 (right). Figure 16 (right) shows no change in overall thickness of the composite layer after thermal cycling. A similar process was followed for sample b106 although we used full-wave CST MWS instead of our faster forward model. The drawback of using full-wave CST MWS is the significant increase in calculation time. In Fig. 16 (left), the estimated thickness is shown over four distinct thermal cycles. The results clearly show a monotonic increase in the thickness of the PE composite as a function of thermal cycling.

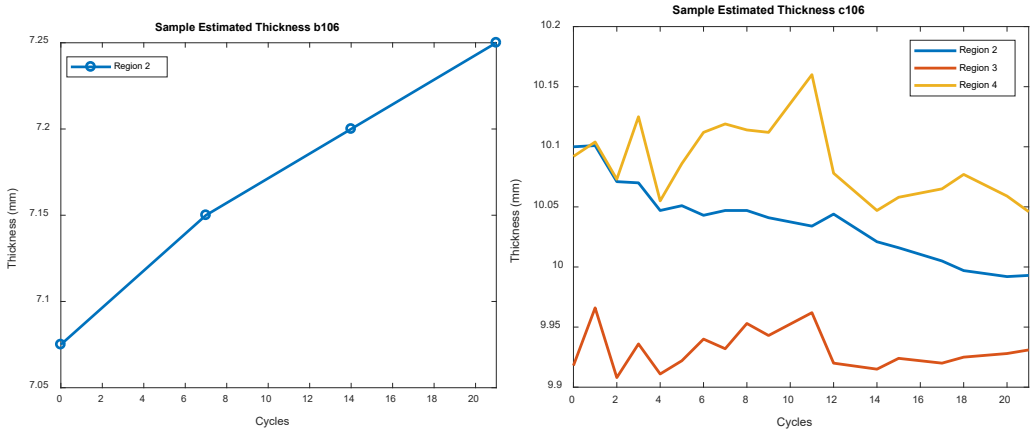

Fig. 16 Calculated thickness using reflection coefficient: (left) b106 sample over 0, 7, 14, and 21 cycles, and (right) c106 sample over all cycles

In practice, any change in the thickness and dielectric properties of the material will reflect as in the measured reflection coefficients. Tracking this change may be a more practical method for inspecting physical changes in the armor. However, a strict measurement procedure must be followed to recreate consistent surface pressure on the foam padding, as the level of pressure changes the reflection coefficient. The difference in reflection coefficient (i.e., error), calculated with reference to the reflection coefficient of the sample prior to thermal cycling and averaged over the measured frequency band and as a function of thermal cycling, is shown in Fig. 17 for samples b105 and b106, respectively. These two samples showed a progressive change in the calculated "error" of the measured reflection coefficient after Cycle 11. These data should be compared with the ground truth data obtained from these samples after thermal cycling. For the covered sample c105, as shown in Fig. 18, the results show changes similar in magnitude to b105, but not in a systematic way. For the uncovered sample c106, there is no change in this parameter as a function of thermal cycling.

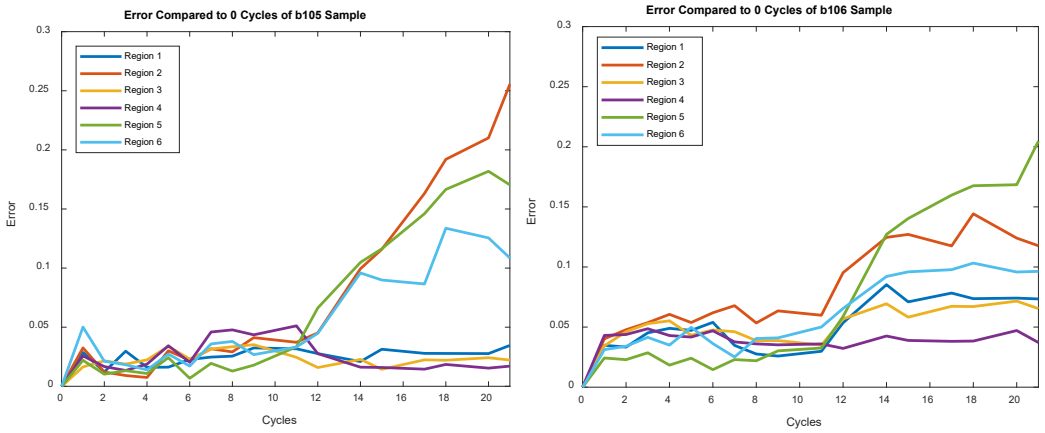

Fig. 17 Difference in reflection coefficient of samples b105 and b106, respectively, plotted as error vs. number of cycles

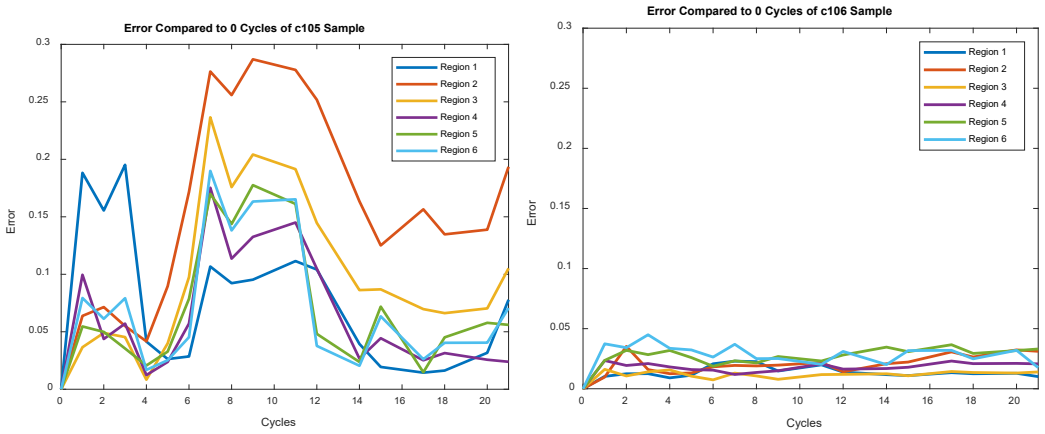

Fig. 18 Difference in reflection coefficient of samples c105 and c106, respectively, plotted as error vs. number of cycles

9. Numerical vs. Measurement Results

As mentioned in Sections 5 and 6, an anomaly was discovered in our simulation using the custom-designed numerical model, called *n-layer*, for one of the armor-layered configurations where the simulation results numerically converged; however, the results did not match those obtained by the measurements or the commercial full-wave simulation software CST MWS. Figure 19 shows an example where the reflection coefficient measurements on an armor sample and the corresponding simulations using CST MWS show similar trends. However, the *n-layer* model results, which simulates an ideal (infinite in extent) multilayered structure, diverge from the measurement and the CST MWS simulation results for about half of the frequencies within the investigated band, in this case Ku-band (12.4–18 GHz). This was contrary to the expectations where the *n-layer* model

always closely predicts the CST MWS simulation results for an ideal multilayered structure. Furthermore, since the measurements were performed using an engineered probe flange (electrically resembling an infinite flange),[19] it too was expected to closely match the *n-layer* results, which also assumes an infinite flange. Initially, this was believed to be due to the *n-layer* model. Having a robust *n-layer* model is essential since it is this model that is at the core of the algorithms used for calculating layered armor properties such as thickness and dielectric properties.[18] As will be shown later, this model actually did not suffer from any numerical or convergence shortcomings, and the main source of this anomaly was the improper setup of the CST MWS simulation model.

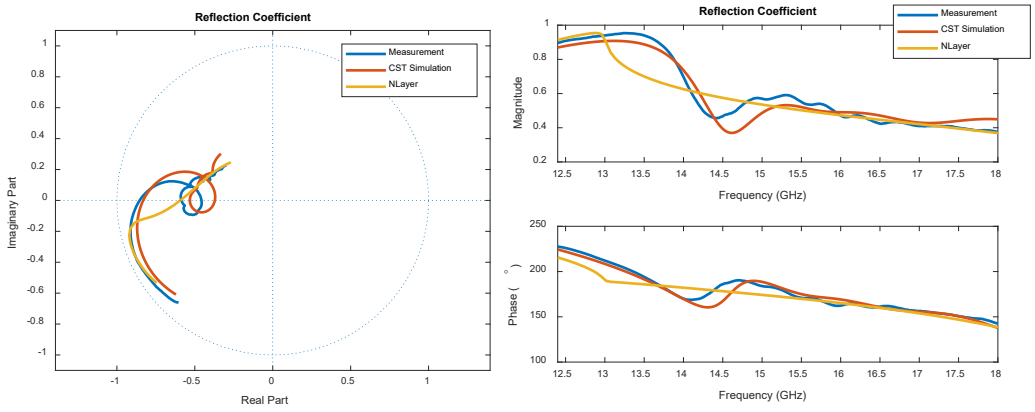

a) b)

Fig. 19 Comparison of the reflection coefficient obtained at Ku-band (12.4–18 GHz) using measurements on an armor sample, full-wave simulation using CST MWS, and the *n-layer* model. Reflection coefficients are plotted a) in the complex plane and b) as magnitude and phase.

To find the source of the aforementioned anomaly (as shown in Fig. 19), the mathematical derivation of the *n-layer* model and the programmed code were extensively reviewed. Several simulations were performed and internal variables of the *n-layer* model were closely inspected. It was discovered that the anomaly occurs when the structure is low-loss, conductor backed (similar to the armor where the ceramic is conductive), and the thickness of the dielectric is about half-wavelength or multiples thereof similar to the tested armor. In this situation, the integrands within *n-layer* exhibit multiple singularities. However, we found that the *n-layer* code properly accounts for and calculates these singularities and no computational errors were found. In the end, it was discovered that *n-layer* had no issues with convergence and the main issue was with the numerical CST MWS simulations, which did not properly model the boundary conditions in an infinitely (in spatial extent) multilayer structure.

Normally, when simulating the reflection coefficient of an infinite (in spatial extent) multilayered structure, it is assumed that CST MWS simulates a sufficient spatial extent of the material to represent an infinite sample. It turns out this size can be quite large in cases where the material is low-loss, conductor backed and when resonances are present. Figure 20 shows the simulation models in CST MWS where an open-ended waveguide probe is used to measure the reflection coefficient when testing an armor piece. In this simulation, the armor and the probe were modeled with slight matching curvatures. As shown in Fig. 20a, finite engineered flanges with rounded edges (mimicking infinite flanges) as used in measurements were simulated in the Ku-band (12.4–18 GHz). Additionally, a truncated, very large flange was also simulated, as shown in Figure 20b. Figure 21 shows the simulation results where the small 60-mm flange, which is the same size as the flange used during measurement, has a similar reflection coefficient as the previous measurement shown in Fig. 19. Further extending the flange to over three times the size (i.e., 210 mm) causes the results to be very similar to those obtained by the *n-layer* model. Similar results were noticed in Kempin et al.[19] where a larger flange provided a better match to the *n-layer* results for conductor-backed structures; however, the differences here are accentuated due to resonances in the structure. Figure 21 also shows that the very large flange, which closely matches the curvature of the sample, more closely matches the *n-layer* model results. In conclusion, either a probe with larger flange may have to be designed and used for measurements, or the measurements must be performed in a frequency band where the structure is not resonant.

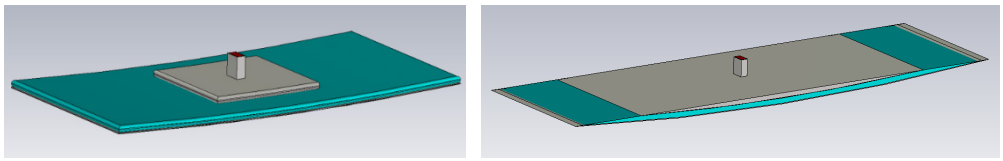

a) b)

Fig. 20 CST MWS simulation models for a) probe with a finite engineered flange with curved edges and b) very large flange matching the curvature of the armor

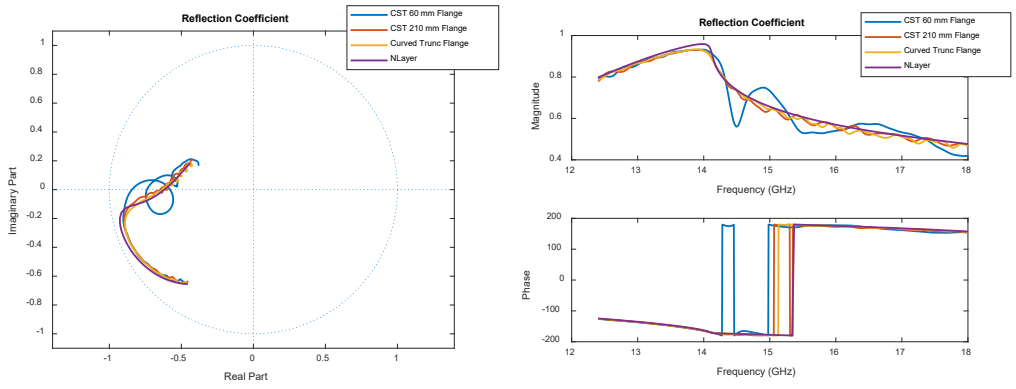

a) b)

Fig. 21 Ku-band (12.4–18 GHz) comparison of the reflection coefficient obtained using full-wave simulation with CST MWS for various flange sizes and the *n-layer* model. Reflection coefficients are plotted a) in the complex plane and b) as magnitude and phase.

10. Effect of Armor Curvature

Another issue investigated was the effect of armor curvature on the measured reflection coefficient. Simulations were performed to estimate the effect of the armor curvature on the reflection coefficient measured by the open-ended waveguide probe. These simulations compared the result obtained from a) probes with curved apertures matching the curvature of the armor, b) probes with flat apertures measuring the curved armor, and c) probes with flat apertures measuring a flat armor (ideal case). The outcomes of these simulations provide a quantitative estimate of the expected error in reflection coefficient measurements, which can then be used to optimize a probe aperture for measuring properties of curved armor structures.

Several simulations were performed to investigate the influence of armor curvature on the measured reflection coefficient. As shown in Figs. 22 and 23, CST MWS simulations were performed to obtain the reflection coefficient of a probe with a flat flange (FF) inspecting a piece of flat armor versus flat and curved probes inspecting a piece of curved armor. Curvature radii of 350 mm and 3500 mm were considered for the armor since the curvature varies drastically even within a single armor piece. It must be noted that for both the flat and curved flange (CF) cases, the flange edges were rounded to further improve their response toward matching an infinite sized flange.[19] Figure 24 shows the magnitude of reflection coefficient results over the K-band (12.4–18 GHz) for the FF probe inspecting a flat armor plate. As expected, when the probe size becomes large, the CST MWS simulation results match the *n-layer* results.

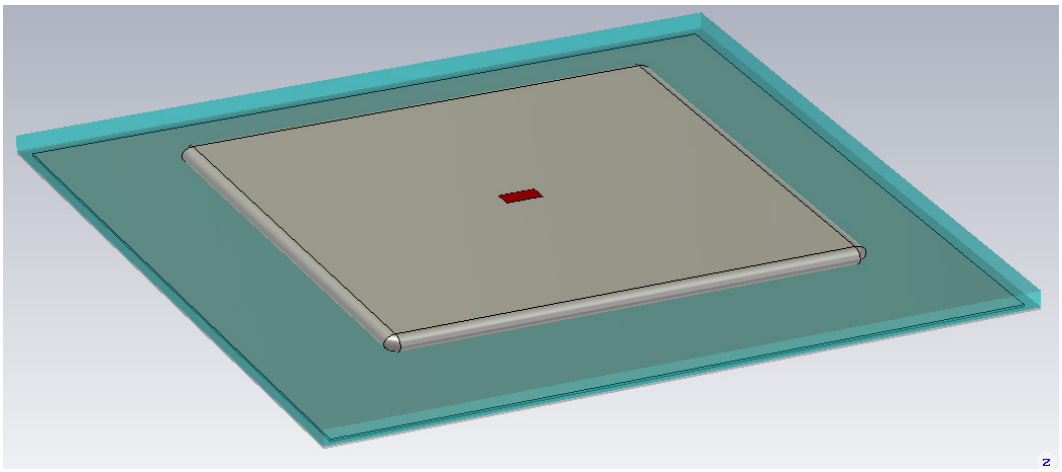

Fig. 22 CST MWS simulation model of a flat flange (FF) probe inspecting a flat sample (FS)

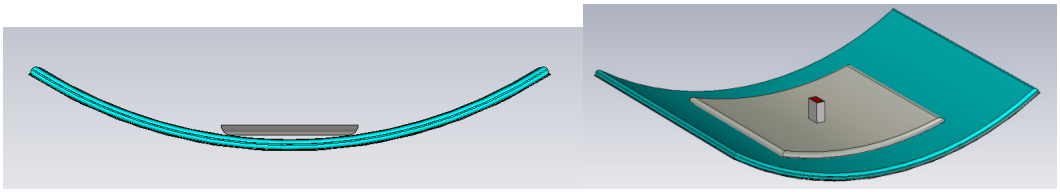

a) b)

Fig. 23 CST MWS simulation model of a) an FF probe and b) a curved flange (CF) probe inspecting a curved sample (CS) with a curvature radius of 350 mm

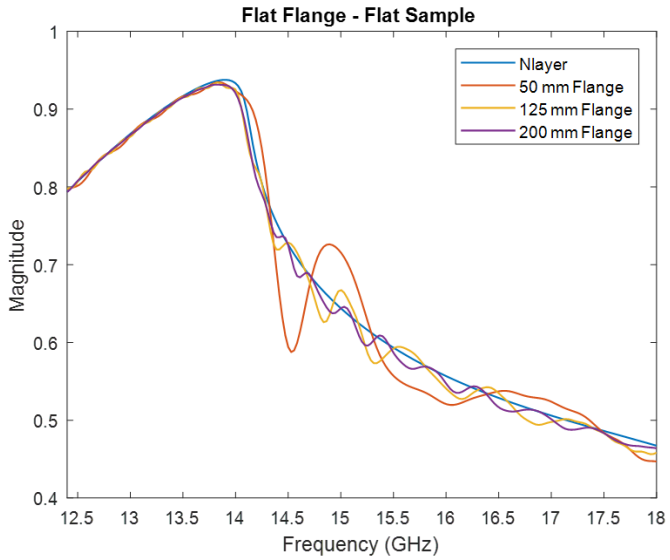

Fig. 24 Magnitude of the reflection coefficient, at K-band (12.4–18 GHz), for the FS using an FF with different sizes

Figure 25 shows the simulation results obtained over the K-band (12.4–18 GHz) using a flat probe on curved armor, as shown in Fig. 23a. These results show that as flange size increases, the reflection coefficient becomes drastically different from the baseline *n-layer* results, as expected. When the curvature is large (i.e., 3500 mm) and the probe is small (i.e., 50 mm) the reflection coefficient results are closer to the *n-layer* results, as expected, but may still not be considered sufficiently close. These large differences are due to the air gap present between the probe and armor as a result of the curvature, as shown in Fig. 23a. When the probe is designed to match the curvature of the sample, as shown in Fig. 23b, the results shown in Fig. 26 are obtained. These results show that when the probe flange matches the curvature of the armor, the reflection coefficient becomes similar to the flat armor and flat probe case, as shown in Fig. 24. In other words, the reflection coefficient is similar to the baseline *n-layer* model regardless of curvature and the match becomes closer for larger probe flanges. Figure 27 shows a summary of these results. Root mean square (RMS) error was calculated between the results obtained from CST MWS simulations and the results from the *n-layer* model, as discussed in Ghasr et al.[17] As expected, the RMS error for the FF and FS case is lowest and reduces with increasing probe flange size since *n-layer* models an infinite flat multilayered structure. This RMS error for the FF and CS are the highest and increases with the curvature (smaller diameter), as expected. Finally, the results for a CF and CSs are low as well, and closely match the baseline *n-layer* case. In conclusion, a practical probe must be designed to closely match the curvature of the sample and be sufficiently large. Further simulations and optimizations are required to arrive at a practical probe for armor inspection.

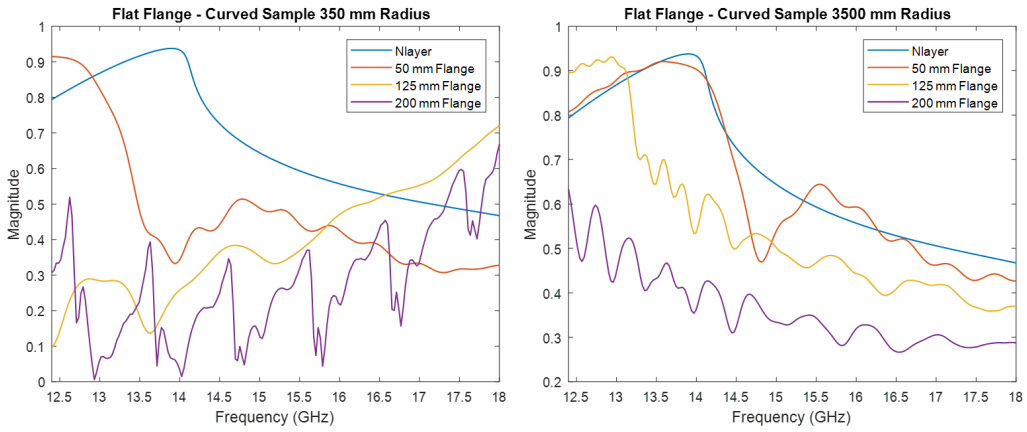

a) b)

Fig. 25 Magnitude of the reflection coefficient, at K-band (12.4–18 GHz) for a) 350- and b) 3500-mm CSs using an FF with different sizes

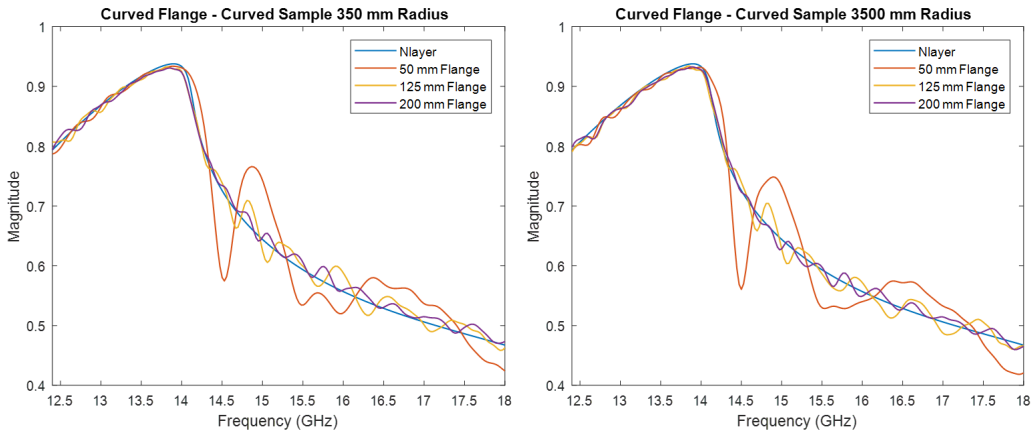

Fig. 26 Magnitude of the reflection coefficient, at K-band (12.4–18 GHz), for a) 350- and b) 3500-mm CSs using a flange with matching curvature and different sizes

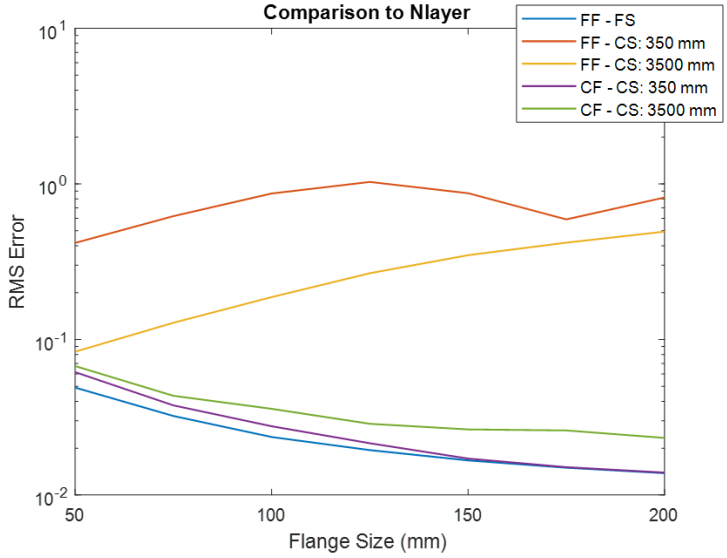

Fig. 27 Difference comparison of the reflection coefficient between the simulated conditions in CST MWS and the *n-layer* model

11. Results of Wideband FM-CW Radar Measurements

Another method for measuring the thickness of a dielectric slab (e.g., composites) is using time-domain reflectometry, similar to an A-scan in ultrasonic testing (UT). Due to the difficulties in creating narrow pulses in microwave and millimeter wave frequency ranges, similar measurements can be performed by using a wideband signal that is swept over the frequency band in a specified amount of time. This is essentially the basis for an FM-CW radar.[23] Thus, by performing wideband frequency domain reflection measurements using a VNA, one can process the data

using Fourier transform processes (in lieu of a frequency spectrum analyzer) and obtain range or thickness information, much like a UT A-scan.

Figure 28 shows schematics for such a measurement method applied to inspecting an armor sample made of a thin padding layer, a composite layer, and a ceramic layer. The ceramic layer is covered in conductive carbon and as such, it acts as a reflector of microwave/millimeter wave energy (i.e., no signal penetration through it). In the inspected armors, the padding layer is very thin (on the order of few millimeters). Additionally, given that the padding is soft, by placing a probe (an open-ended rectangular waveguide) on top of it, it compresses and thus its thickness changes depending on the amount of pressure applied. One of the difficulties in using this method is the required large transmitted signal bandwidth since range, or in this case thickness, resolution is inversely proportional to this bandwidth. Range or thickness resolution is strictly a function of transmitted signal bandwidth and is equal to ($\sim v_p/2B$), where v_p is the signal phase velocity. In air, v_p is equal to the speed of light (c) and in a dielectric material, it is reduced by a factor of $(\varepsilon_r')^{-0.5}$, which makes the resolution in a dielectric material (i.e., composite in the armor) finer by this factor. Thus, the thin padding layer and not having sufficient signal bandwidth will translate to not being able to distinguish between the reflections from the probe aperture, shown as the red arrow in Fig. 28, and the reflection from the top of the composite (the first blue arrow in Fig. 28). Thus, the thickness of the composite layer (distance between the two blue arrows) cannot be estimated accurately. Figure 29 shows an alternative configuration where two probes are used in a bi-static configuration. Using this approach, the received signal from the top of the padding (the red arrow) is greatly reduced in strength at the expense of slightly overestimating the thicknesses (longer signal travel path). Using these methodologies, measurements were performed on an armor sample 28520 from LTC using open-ended waveguide probes over the Ka-band (26.5–40 GHz). At this frequency and in air, the range/thickness resolution is approximately 11.1 mm, and it is approximately 7.5 mm in the PE composite (as per Table 1).

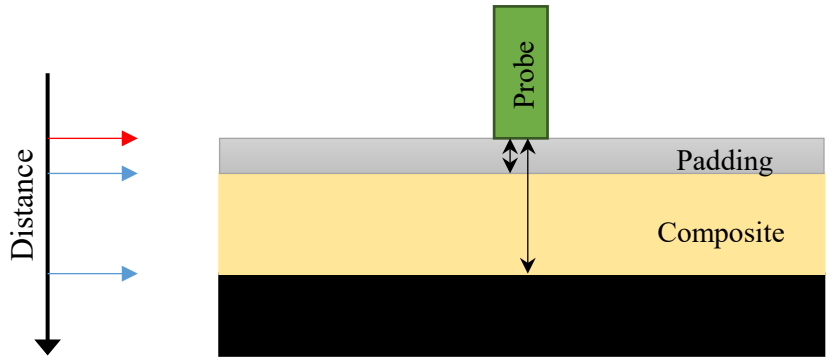

Fig. 28 Mono-static (single probe) configurations for measuring dielectric thickness

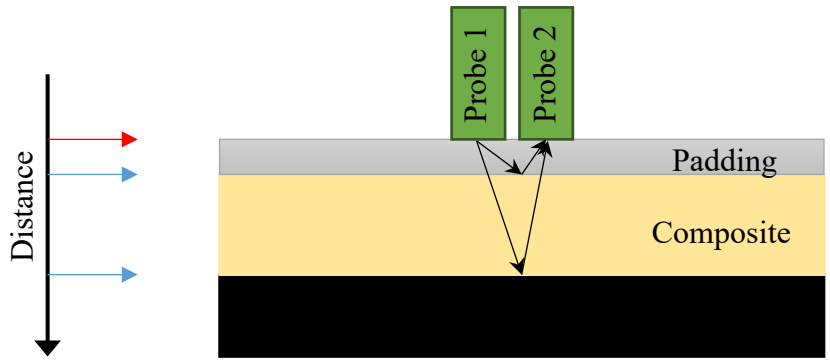

Fig. 29 Bi-static (dual probe) configurations for measuring dielectric thickness

Six measurements were performed over different areas of the sample's inner surface. Figure 30 shows the results for the six measurement locations using the mono-static (single-probe) method. The reflections from the top and bottom of the padding merge into a wide peak near x = 0 mm. As such, the distance between this wide peak and the peak near the distance of x = 15 mm is not an accurate representation of the actual composite thickness. Figure 31 shows the results of the bi-static measurements, where two distinct peaks at distances of 2.77 and 13.5 mm are observed. These peaks correspond to the top and bottom reflections of the composite only and as such, the difference between them (~10.7 mm) corresponds to the thickness of the composite in this sample (0.42 inch). For generating these curves and estimating the distances accurately, the relative dielectric permittivity of the composite (ε_r = 2.3) was considered, as per the data in Table 1 for PE composite.

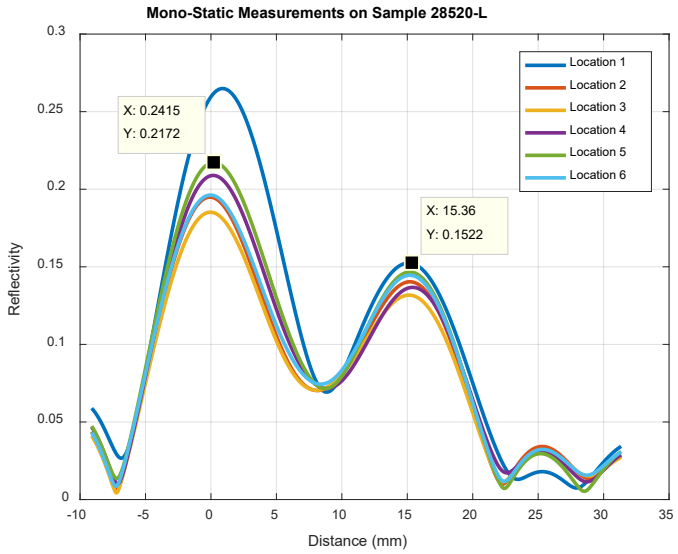

Fig. 30 Thickness measurement results for the 28520 sample using the mono-static method

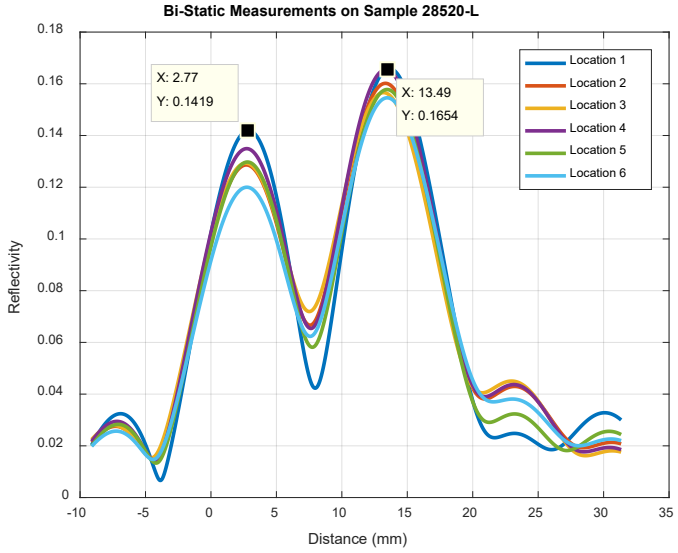

Fig. 31 Thickness measurement results for the 28520 sample using the bi-static method

Larger signal bandwidth, such as those possible over the V-band (50–75 GHz) or W-band (75–110 GHz) frequency ranges, will provide better thickness estimations on larger varieties of samples. Thus, simulations were also performed using CST MWS for a bi-static W-band (75–110 GHz) dual probe for measuring the thickness of the PE composite when covered by the foam padding. The signal reflectivity versus distance results are shown in Fig. 32 where the peak near a distance from the surface of 3.46 mm corresponds to the top of the PE composite (the bottom of the foam padding). The bandwidth associated with W-band provides a range resolution of approximately 4.3 mm in air and approximately 2.8 mm in the PE

composite (as per Table 1). Since foam has a dielectric constant similar to air, the resolution is not sufficient to isolate the top and bottom reflections of the foam. However, the bi-static configuration removes the reflection from the top of the foam (at the distance of 0 mm), as explained previously. The results show that the reflection at the top of the PE composite (bottom of foam) is clearly detected at a distance of approximately 3.46 mm, while the reflection from the bottom of the composite is shown as a strong peak that moves in distance (to the right in Fig. 32) as a function of increasing PE composite thickness. The thickness of the PE composite (for each curve) is thus measured as the distance between these two peaks. These results further show the efficacy of this technique for PE composite thickness measurement.

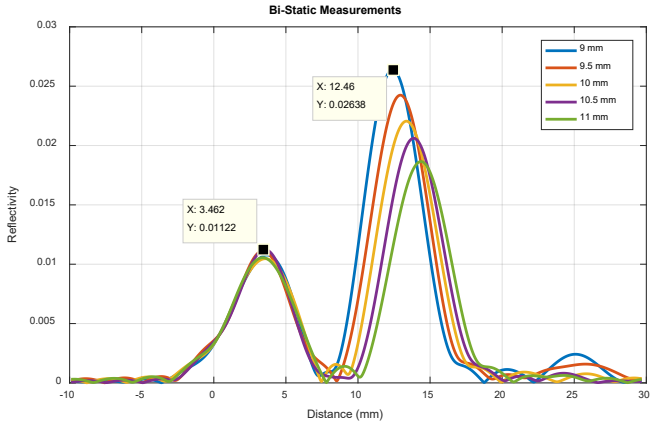

Fig. 32 Simulated results for thickness estimation of PE composite using a bi-static W-band ranging probe

12. Handheld VNA and Custom User-Interface Software for Material Characterization

In Phase I, we spent significant effort developing a fieldable inspection system. This entailed several discussions with VNA manufacturers, evaluating available end effectors at the frequency of interest, testing different connection approaches, and testing hardware functionality on the LTC panels.

The prototype developed in Phase I is shown in Fig. 33. It includes a COTS VNA, an end effector to shape and direct the microwave energy, a custom-designed and manufactured waveguide flange to prevent reflections and reduce noise, custom software to assist in system calibration, data collection, data display, data archiving, and data analysis, and a laptop to run the software and store data.

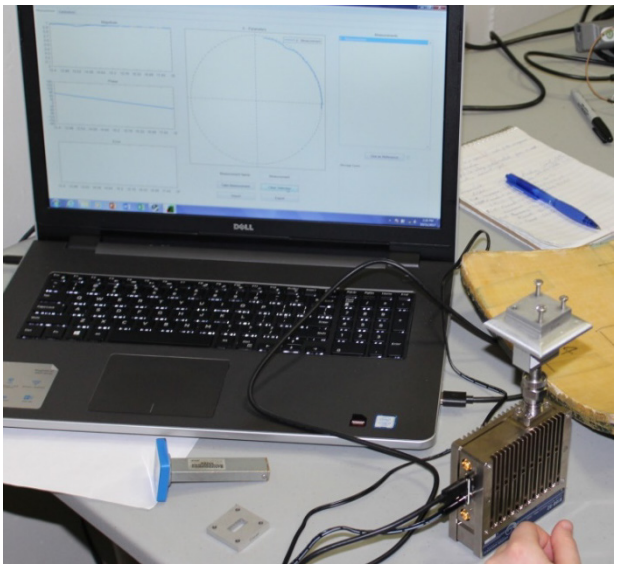

Fig. 33 Microwave NDT device (lower right) and laptop computer running data collection software at ARL

The handheld Copper Mountain VNA is an easy-to-use vector reflectometer that can provide accurate measurements for material characterization purposes. Figure 34 shows the R180 vector reflectometer attached to the custom open-ended waveguide probe (mentioned earlier) inspecting an LTC armor sample. Although the R180 is an easy-to-use device, its user-interface software is developed for the telecom industry and does not allow data analysis for material characterization or waveguide calibration. We developed a user-interface software, shown in Fig. 35, which provides a guided calibration routine, ability to save/recall calibration data, and the ability to record reflection coefficient data and save these data to a file. Furthermore, the user-interface software allows the user to monitor changes in the reflection coefficient data, such as changes due to thermal cyclic aging.

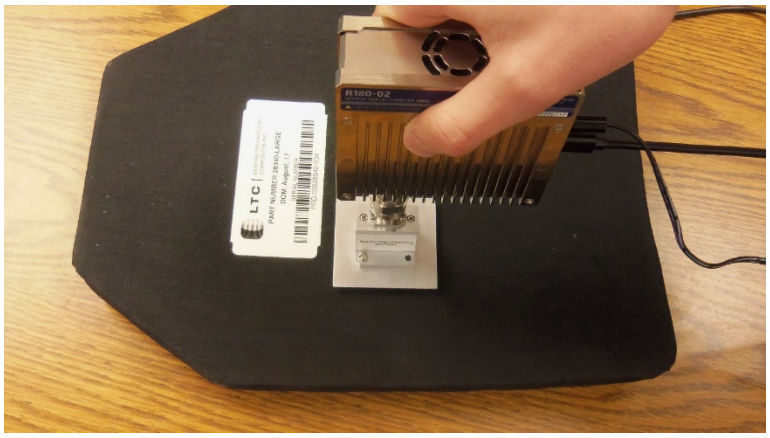

Fig. 34 R180 vector reflectometer from Copper Mountain Technologies being used to inspect an armor sample using the patented open-ended waveguide probe

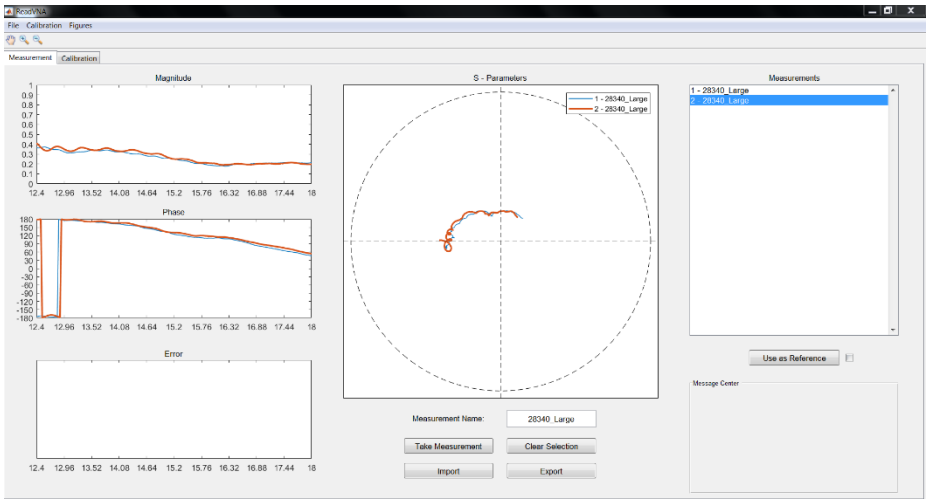

Fig. 35 User interface developed by the Missouri University of Science and Technology research team for calibrating and obtaining reflection coefficient data from the R180, analyzing the data for changes in reflection coefficient, and saving the data

13. Commercialization

We were aware of an X-ray system manufactured to inspect the ceramic part of body armor plates so we wanted to investigate the sales of those systems. Since our system inspects the polymer composite part of the plates, we expect our system will be complementary to the X-ray system and companies selling these systems may be targets to market and sell the microwave NDT system to. We discovered an X-ray system made by J D L L, Inc. of Midvale, UT (Cage Code 3DQ34). The system is called the AIS-NDTE, where AIS can refer to armor inspection system or automated inspection system and NDTE refers to nondestructive test and

evaluation. The national item identification number is 015702863 and part number is 174031. Each system sells for over $500,000 ($521,456 as of 2017).

We were not able to identify exactly where all the X-ray systems are located, but some locations are in:

- Barstow, California
- Camp Lejeune, North Carolina
- Camp Pendleton, California
- Cheatham Annex, Virginia
- Kaneohe, Hawaii
- Okinawa, Japan
- Rhine Ordnance Barracks, Kaiserslautern, Germany

14. Summary and Conclusions

Overall, we believe this investigation demonstrates microwave NDE can detect degradation in the composite backers on armor plates. Based both on the Phase I effort and previous work by the research team on measuring thickness of layers in stacks, we also feel confident that our approach can be used to measure thickness of the composite backer. We also are confident the Phase I prototype field testing shows the technique can be done in a rugged, fieldable, easy-to-use system.

There are obviously improvements that need to be made before fielding a microwave NDE device for armor. For example, automating calibration, or better yet, making the system self-calibrating, would improve the system. We need to develop a way to get the system to operating temperature in a couple of minutes instead of 20 min. A simple internal heater would do this, and in the ARL field trials we discovered that simply leaving it in its box (closed) reduced warm-up time. There also needs to be some kind of force indicator or bracket added so that various users consistently apply the same pressure. This would reduce compressing the foam in different amounts by different users. The software needs to be improved to help automate data collection and to provide the operator with an easier-to-interpret result. The hardware can be miniaturized and ruggedized, in particular, the computer.

The biggest effort that needs to be done is correlating thermal aging (and probably other aging mechanisms) to reductions in ballistic performance, and ballistic performance to NDE data.

Through simulations it was shown that for half-wavelength-thick, low-loss multilayered structures backed by a conducting plates, such as one of the two configurations of inspected armor in the Phase I effort, a larger probe flange is needed to perform accurate measurements matching the theoretical *n-layer* model. Additionally, it was shown that the probe flange needs to closely match the armor curvature to provide measurements that match the *n-layer* model results. Frequency of operation may need to be changed and/or flange size and geometry may need to be optimized to arrive at a practical design for armor inspection. This design and optimization will be completed during the Phase II endeavor.

Finally, Phase I work included wideband FM-CW radar results that show significant potential for measuring PE composite thickness. This is a relatively simple measurement and the results are a direct measurement of the thickness. The primary difficulty in fielding this system is scarcity of equipment that operates above 40 GHz. Before pursuing this approach, we would research vendors and component suppliers to ensure we could develop an affordable, fieldable system.

15. References

1. Body Armor News. Harford testing firm unveils new CT X-ray scanner. 2012 Mar 19 [accessed 2019 Aug 21]. https://www.bodyarmornews.com/harford-testing-firm-unveils-new-ct-x-ray-scanner/.

2. Textile World. TenCate acquires Smart Body Armor® technology from Newport Sensors. 2014 Oct 13 [accessed 2019 Aug 21]. https://www.textileworld.com/textile-world/nonwovens-technical-textiles/2014/10/tenccate-acquires-smart-body-armor-technology-from-newport-sensors/.

3. Serna J. Sensing protection issues. Daily Pilot. 2008 Jan 2.

4. Stewart C. Ceradyne backs Maria Feng's UCI research on armor defects. OC Register. 2008 Jan 4.

5. Acoustic emission (AE) technology. Princeton Junction (NJ): Physical Acoustics Corporation. c2019. [accessed 2019 Aug 21]. http://www.physicalacoustics.com/ae-technology/.

6. Swiderski W, Szabra D, Szudrowicz M. Nondestructive testing of composite armours by using IR thermographic method. QIRT 2008. 9th International Conference on Quantitative InfraRed Thermography; 2008 July 2–5; Krakow, Poland. http://www.ndt.net/article/qirt2008/12_12_16.pdf.

7. Van Den Abeele K, Sutin A, Carmeliet J, Johnson PA. Micro-damage diagnostics using nonlinear elastic wave spectroscopy (NEWS). NDT&E Int. 2001;34(4):239–248.

8. Van Den Abeele K, Johnson PA, Sutin A. Nonlinear elastic wave spectroscopy (NEWS) techniques to discern material damage, part I: nonlinear wave modulation (NWMS). Res Nondestruct Eval. 2000;12(1):17–30.

9. Ulaby FT, Moore RK, Fung AK. Microwave remote sensing, active and passive–volume III, appendix E. Norwood (MA): Artech House Inc.; 1986.

10. Zoughi R. Microwave nondestructive testing and evaluation. The Netherlands: KLUWER Academic Publishers; 2000.

11. Balanis CA. Advanced engineering electromagnetics. New York (NY): John Wiley and Sons; 1989.

12. Bakhtiari S, Ganchev S, Qaddoumi N, Zoughi R. Microwave non-contact examination of disbond and thickness variation in stratified composite media. IEEE T Microw Theory. 1994;42(3):389–395.

13. Bakhtiari S, Ganchev S, Zoughi R. Microwave frequency optimization for accurate thickness or dielectric property monitoring of conductor backed composites. Mater Eval. 1993;51(6):740–743.

14. Bakhtiari S, Ganchev S, Zoughi R. Open-ended rectangular waveguide for nondestructive thickness measurement and variation detection of lossy dielectric slabs backed by a conducting plate. IEEE T Instrum Meas. 1993;42(1):19–24.

15. Ganchev S, Qaddoumi N, Ranu E, Zoughi R. Microwave detection optimization of disbond in layered dielectrics with varying thicknesses. IEEE T Instrum Meas. 1995;44(2):326–328.

16. Bois K, Benally A, Zoughi R. An exact multimode solution for the reflection properties of an open-ended rectangular waveguide radiating into a dielectric half-space: forward and inverse problems. IEEE T Instrum Meas. 1999;48(6):1131–1140.

17. Ghasr M, Simms D, Zoughi R. Multimodal solution for a waveguide radiating into multilayered structures—dielectric property and thickness evaluation. IEEE T Instrum Meas. 2009;58(5):1505–1513.

18. Fallahpour M, Kajbaf H, Ghasr MT, Case JT, Zoughi R. Simultaneous evaluation of multiple key material properties of complex stratified structures with large spatial extent. Proceedings of the Review of Progress in Quantitative Nondestructive Evaluation; 2011 July 17–22; Burlington, VT.

19. Kempin M, Ghasr MT, Zoughi R. Modified waveguide flange for evaluation of stratified composites. IEEE T Instrum Meas. 2014;63(6):1524–1534.

20. Zoughi R, Gallion JR, Ghasr MT. Accurate microwave measurement of coating thickness on carbon composite substrates. IEEE T Instrum Meas. 2016;65(4):951–953.

21. Shinde S, Jothibasu S, Ghasr MT, Zoughi R. Wideband microwave reflectometry for rapid detection of dissimilar & aged ICs. IEEE T Instrum Meas. 2017;66(8):2156–2165.

22. Gao Y, Zoughi R. Millimeter wave reflectometry and imaging for noninvasive diagnosis of skin burn injuries. IEEE T Instrum Meas. 2017;66(1):77–84.

23. Ulaby FT, Moore RK, Fung AK. Microwave remote sensing, active and passive–volume II, chapter 7. Norwood (MA): Artech House Inc.; 1986.

Appendix. Kickoff Meeting

The kickoff meeting was held 28 June 2017 from 9:30 AM to 1 PM EST. Attendees included:

Russell Austin	Texas Research Institute	In person
Tyrone Jones	US Army Research Laboratory (ARL)	In person
Brian Scott	ARL	In person
Michael Pohland	US Army Materiel Systems Analysis Activity (AMSAA)	In person
Reygan Freeney	US Army Test and Evaluation Command (ATEC)	In person
Aldo Bellotti	NLA Diagnostics	In person
Reza Zoughi	Missouri University of Science & Tech	Teleconference
Tayeb Ghasr	Missouri University of Science & Tech	Teleconference
Troy Goldhammer	CRI Rugged	Teleconference

An electronic copy of the kickoff slides was provided in the first monthly report of this contract.

On 29 October 2017, Russell Austin traveled to Aberdeen, Maryland, so inspection of panels at ARL could begin the morning of 30 October.

On the 30th, Mr Austin met with ARL representatives at the ARL Vehicle Technology Directorate in Building 4603.

Nondestructive test data were collected on as-received (not thermally cycled) armor panels c105, c106, b105, and b106. Panels "b" were made by one manufacturer and "c" by another manufacturer. The 105 panels were complete. The 106 panels were the same models as the 105 panels, but with outer fabric and padding removed to facilitate easy inspection.

On 8 November 2017, Russell Austin left ARL to return to Austin. He collected all data through Cycles 12. Before leaving, he trained ARL staff on system calibration and data collection. ARL staff collected data for Cycles 14, 15, 17, 18, 20, and 21.

All raw data collected during the trip was provided to the Army in an Excel file in December 2017.

List of Symbols, Abbreviations, and Acronyms

AIS	Armor Inspection System
ARL	Army Research Laboratory
CCDC	US Army Combat Capabilities Development Command
CF	curved flange
COTS	commercially available off the shelf
CS	curved sample
CST MWS	CST Microwave Studio
CT	computed tomography
DAC	Data & Analysis Center
ESAPI	Enhanced Small Arms Protective Insert
FF	flat flange
FM-CW	frequency-modulated continuous-wave
FS	flat sample
IR	infrared
LTC	Leading Technology Composites
NDI	nondestructive inspection
NDT	nondestructive testing
PE	polyethylene
PN	part number
RF	radio frequency
RMS	root mean square
SAPI	Small Arms Protective Inserts
SBIR	Small Business Innovation Research
SLAD	Survivability/Lethality Analysis Directorate
TRI Austin	Texas Research Institute Austin, Inc.
UHMWPE	ultra-high-molecular-weight polyethylene

UT	ultrasonic testing
VNA	vector network analyzer

1 (PDF) DEFENSE TECHNICAL INFORMATION CTR DTIC OCA

1 (PDF) CCDC ARL FCDD RLD CL TECH LIB

1 (PDF) TEXAS RESEARCH INSTITUTE AUSTIN INC D MOTES

1 (PDF) ZHENG CONSULTING J ZHENG

1 (PDF) SCOTT CONSULTING B SCOTT

1 (PDF) COORSTEK R PALICKA

1 (PDF) KEYENCE M LAMARRE

1 (PDF) SILSBY CONSULTING G SILSBY

1 (PDF) NATIONAL CENTER FOR MANUFACTURING SCIENCES C BOSWELL-KOLLER

1 (PDF) APPLIED RESEARCH LABORATORY, PENNSYLVANIA STATE UNIVERSITY D SWANSON

1 (PDF) HOTEND WORKS B BECKER

1 (PDF) HP WHITE R KINSLER

2 (PDF) CHESAPEAKE TESTING JB JENNINGS J MARTIN

1 (PDF) PEO SOLDIER SFAE SDR SPIE D OTTERSON

1 (PDF) SOCOM HQ FCDD SCS PS M CLARK

1 (PDF) USSOCOM/SOF AT&L-ST C LOVELL

1 (PDF) CCDC RDCB DEE K WALLACE

1 (PDF) CCDC HEADQUARTERS FCDD CG CT WINS

1 (PDF) CCDC AFRC CIE JJ GALLIVAN

1 (PDF) MEDCOM USAMRDC FCMR ZA MJ TALLEY

3 (PDF) NATICK SSC FCDD SCP WI M ROTH RDNS WDE MM MJ HURLEY RDNS SES WI M MAFFEO

25 (PDF) CCDC ARL FCDD RLD H MAUPIN FCDD RLC NS G WEAVER FCDD RLW S KARNA A RAWLETT S SCHOENFELD J ZABINSKI FCDD RLW P D HOGGE FCDD RLW L T SHEPPARD FCDD RLW M B LOVE FCDD RLW B J CAMPBELL L VARGAS-GONZALEZ C HOPPEL FCDD RLW ME J LASALVIA S SILTON FCDD RLW P R FRANCART FCDD RLW PA S BILYK

FCDD RLW PB
M KLEINBERGER
S SATAPATHY
FCDD RLW PC
D CASEM
J CLAYTON
M FERMEN-COKER
FCDD RLW PD
J RUNYEON
FCDD RLW PE
T JONES
P SWOBODA
FCDD RLW PG
N GNIAZDOWSKI